Hardware-in-the-Loop Simulations and Control Design for a Small Vertical Axis Wind Turbine

Ugur Sancar, Aykut Ozgun Onol, Ahmet Onat, *Member*, IEEE, Serhat Yesilyurt, *Senior Member, IEEE*

Mechatronics Engineering Program
Sabanci University
Istanbul, Turkey
{ugursancar,onol,onat,syesilyurt}@sabanciuniv.edu

Abstract— **Control design plays an important role in wind energy conversion systems in achieving high efficiency and performance. In this study, hardware-in-the-loop (HIL) simulations are carried out to design a maximum power point tracking (MPPT) algorithm for small vertical axis wind turbines (VAWTs). Wind torque is calculated and applied to an electrical motor that drives the generator in the HIL simulator, which mimics the dynamics of the rotor. To deal with disturbance torques in the HIL system, a virtual plant is introduced to obtain an error between the speeds in the HIL system and virtual plant. This error is used by a proportional-integral (PI) controller to generate a disturbance torque compensation signal. The MPPT algorithm is tested in the HIL simulator under various wind conditions, and the results are compared with numerical simulations. The HIL simulator successfully mimics the dynamics of the VAWT under various wind conditions and provides a realistic framework for control designs.**

Keywords—Hardware in the loop; maximum power point tracking; vertical axis wind turbine, inertia emulation; disturbance torque compensation

I. INTRODUCTION

Renewable energy systems are very popular due to increasing energy demand in the developing world, the climate-change threat and diminishing reserves of fossil fuels. The widespread use of wind energy is enabled in part by horizontal axis wind turbines (HAWTs) even though they were invented later than VAWTs, which are viable alternatives in the small scale use of wind energy as they are omnidirectional and have simpler designs than HAWTs [1,2]. Moreover, VAWTs can be used as portable generators in rural areas and connected to local micro grids and storage devices. Cost effective system design of VAWTs bears utmost importance for their ubiquitous deployment.

Power electronics is used to control and regulate the torque and speed of wind turbines in order to maximize the power output [3]. For VAWTs with fixed pitch angles, extracted wind power can be characterized by a power coefficient, which is a function of the rotor angular velocity and wind velocity and denoted by C_p [4]. For a particular wind velocity, the turbine needs to be driven at the optimal rotor speed to operate the system at maximum power [5]. Variants of the maximum power point tracking (MPPT) algorithms are present in the literature and can be classified into two categories [6]: MPPT based on knowledge of rotor dynamics, and MPPT based on an iterative incremental search. In order to reduce the cost of small-scale applications, a sensorless MPPT method is preferred for the optimum operation of the system in terms of energy efficiency since knowledge of the turbine parameters and measurement of the wind and rotor speeds are not required [7,8].

Hardware-in-the-loop (HIL) simulations have numerous advantages over numerical, i.e. only software based, simulations in testing the performance of power electronic components and control designs in controlled experiments under realistic conditions [9]. The effects of generator parameters, the sampling period of control units, thermal effects and other disturbances are observed directly in HIL simulations [10]. Types of HIL designs are discussed in detail by Bouscayrol [10]; here we employ a mechanical level HIL simulator to study the efficiency of MPPT algorithms in the control of a permanent magnet generator that is used in a small-scale VAWT. In order to ensure the fidelity of the simulator, the static and dynamic characteristics of the HIL simulator must be the same as the characteristics of the real system [11].

The motor in the HIL simulator can deliver the wind torque and inertial torque of the rotor with the help of a compensation torque and by calculating the speed derivative as previously reported by [11-13]. However, for an accurate estimation of the speed derivative, a low-pass filter (LPF) may be necessary to eliminate the measurement noise. Moreover, filtering the speed or its derivative introduces delays which impede accurate mimicking of the VAWT system and successful implementation of the control algorithm. In order to alleviate the difficulties associated with delays, one can propose a closed-loop observer to calculate the derivative of the angular velocity and reject the noise as in [14], or alternatively, estimation of the speed derivative and the use of the LPF can be eliminated by using the similarity between the real system and the HIL system dynamics as described in Section II-B. In this work, electromechanical components in the HIL simulator are tested at steady-state and transient conditions to confirm the accurate representation of the small VAWT, then the MPPT algorithm is applied to study the effects of the sampling period and current increments. Comparisons are presented between the HIL simulations (HILS) and numerical simulations based on a power coefficient curve and the dynamics of the rotor.

II. METHODOLOGY

A. Aerodynamic Model of the VAWT

The available wind power of a VAWT of radius R and length L is given by:

$$P_{wind} = C_p \rho L R U_w^3 \tag{1}$$

where ρ is the air density, U_w is the wind speed, C_p is the power coefficient, which is a function of tip speed ratio, λ, which is given by:

$$\lambda = \frac{\omega_r R}{U_w} \tag{2}$$

where ω_r is the rotor angular velocity. In this study, a $\lambda - C_p$ curve that is obtained by using a computational fluid dynamics simulation is employed (Fig. 1).
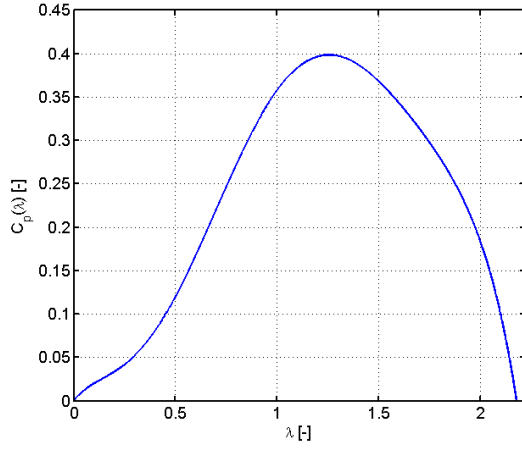

Fig. 1. $\lambda - C_p$ curve of the VAWT.

The wind torque, T_{wind}, is calculated from (1) and the angular velocity of the rotor, ω_r:

$$T_{wind} = \frac{P_{wind}}{\omega_r} = \frac{C_p \rho L R U_w^3}{\omega_r} \tag{3}$$

The dynamic model of the wind turbine can be represented by

$$J_r \frac{d\omega_r}{dt} = T_{wind} - T_{gen} - T_{rf} \tag{4}$$

where J_r is the equivalent inertia of the rotor, T_{gen} is the generator torque on the rotor, T_{rf} is the rotor friction torque, which is assumed to be proportional to ω_r by a coefficient B as follows:

$$T_{rf} = B\omega_r \tag{5}$$

Parameters of the VAWT model are given in Table I.

TABLE I. Wind Turbine Model Parameters

Wind Turbine Model Parameters			
Parameter	*Description*	*Value*	*Unit*
J_r	Moment of inertia of the rotor	2	kg-m^2
R	Radius of the rotor	0.5	m
L	Length of a blade	1	m
B	Friction coefficient	0.02	Ns/rad
ρ	Air density	1.2	kg/m^3

B. Hardware-In-the-Loop (HIL) System

Schematic representation of the VAWT and HIL systems are shown in Fig. 2. The HIL system consists of a permanent magnet synchronous motor (PMSM) (Femsan 5F100810001), a motor drive (TDE Macno, Mopde B-6.8A) and a gear box (Yilmaz Reduktor MN002 – B07) to reduce the velocity of the motor that mimics the wind-driven rotor under arbitrary wind conditions. Additionally, a permanent magnet synchronous generator (PMSG) which is also considered for actual VAWT system, and a programmable electronic load (Agilent N3306A) as the power sink are employed in the HIL system. As an interface between software (MATLAB/Simulink) and hardware, dSpace (DS1104) controller card is used.
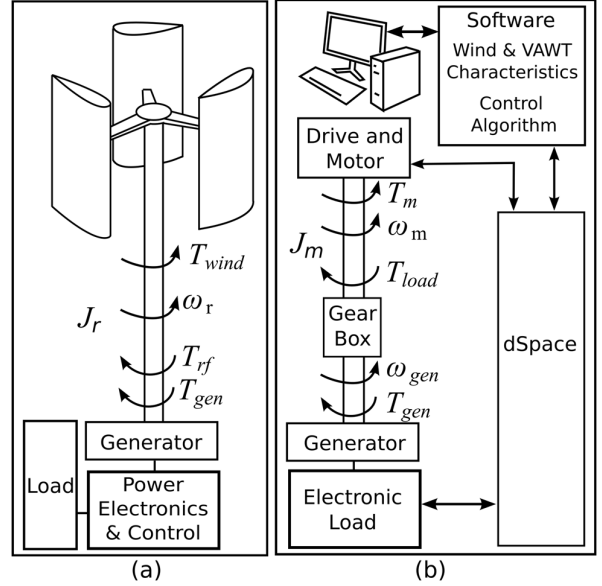

Fig. 2 (a) Representation of VAWT system in real world, (b) HIL simulation system.

The rotor dynamics of the VAWT system in Fig. 2(a) is given by (4). The same dynamic behaviour can be mimicked by the HIL system with the equation of motion at the motor side:

$$J_m \frac{d\omega_m}{dt} = T_m - T_{load} \tag{6}$$

where T_m is the motor torque, ω_m is the rotational speed of the motor shaft, J_m is the equivalent inertia at the motor side of the gear box, and the total load torque, T_{load} is given by:

$$T_{load} = \frac{T_{gen}}{\Gamma} + T_{hf} \tag{7}$$

where T_{gen} is the torque of the generator, Γ is the gear ratio and T_{hf} is the friction torque, which corresponds to the friction in all components including the gear box, generator and motor. The rotational speed of the generator, ω_{gen}, is linked to the motor speed by (8).

$$\omega_{gen} = \frac{\omega_m}{\Gamma} \tag{8}$$

Assuming that the VAWT does not have a gear box and the generator is directly coupled to the rotor, the rotational speed of the

rotor is the same as the rotational speed of the generator in the HIL system, i.e., $\omega_r = \omega_{gen}$. Thus, the behaviour of the VAWT system can be mimicked by the HIL simulator with the appropriate motor torque T_m, which is applied as a reference torque in the HIL simulator and calculated from (4), (6), (7), and (8) as follows:

$$T_m = T_{load} + \frac{J_m \Gamma}{J_w}(T_{wind} - T_{gen} - T_{rf}) \qquad (9)$$

The block diagrams of the VAWT system and the HIL system are given in Fig. 3 where the motor is the actuator and used for mimicking the rotor dynamics in the HIL system. As shown in Fig. 3 and from (9), the load torque, T_{load}, is employed in the reference motor torque calculation, and T_{load} is calculated by using the generator torque, T_{gen}, and friction torque, T_{hf}, as in (7). Consequently, if the generator and friction torques in the HIL system are known, a perfect cancelation of T_{load} can be achieved. In this way, the generator angular velocity, ω_{gen}, behaves in the same way as in the VAWT system. However, neither the generator nor the friction torques are easy to obtain precisely. For permanent magnet synchronous machines, there is a cogging torque, furthermore, the relation between the current and torque is not purely linear [15]. Furthermore, nonlinear friction torque may lead to difficulties. Compensation for the friction torque can be achieved by model-based or non-model-based methods as described in [16].
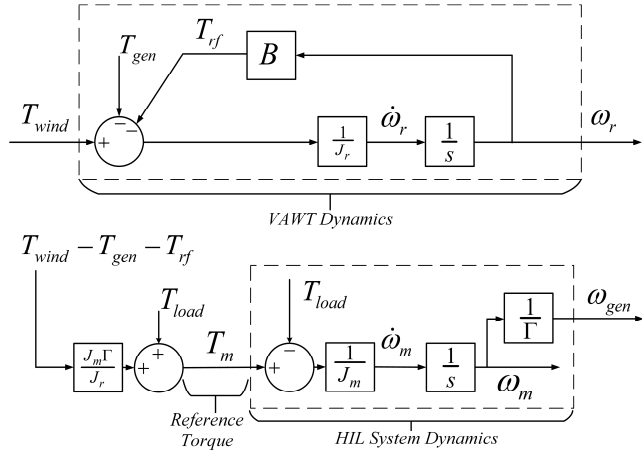

Fig. 3. Block diagram of the VAWT dynamics, HIL System and reference motor torque calculation.

In the non-model-based compensation approach, the friction torque is treated as a disturbance for the system and can be compensated by the disturbance observer (DO) [17]. Derivatives of the angular velocity can be filtered in the DO to eliminate the noise, which influences the derivatives dramatically. A high gain LPF provides a fast disturbance rejection performance. However, if a low-cost sensor (resolver) is used to measure the speed, relatively large noise at low speeds limits the gain, introduces a delay, and distorts the characteristics of the system. Hence, the disturbance torque cannot be fully compensated in a robust manner. Several approaches to deal with this problem are

proposed in literature: rapid disturbance changes in DO structures are discussed and a virtual plant model-based control is proposed to deal with disturbance torques in [18]; in addition to a virtual-plant disturbance compensator a friction-model-based feed-forward compensator is proposed in [19].

In this study, not only the friction torque, but also the deviations from the linear relationship between the torque and the current on the generator side and all other external effects are treated as disturbances. First, the friction torque is obtained by using curve-fitting for the load-free motor torque and speed measurements. Then, the generator torque, T_{gen}, in the HIL system is obtained from the motor and friction torques for a given speed and current, and the torque constant is obtained. Moreover, the virtual-plant model is used to obtain the error between the actual speed and the speed in the virtual-plant model. The virtual plant is identical with the dynamic model of the wind turbine expressed by (4). This equation is applied in the virtual plant block to determine the rotor speed as a function of the total torque in the lack of external effects. The difference between the speed generated by the virtual plant (ω^*_{gen}) and the actual speed (ω_{gen}) is the error that is used to generate the disturbance compensation torque by a PI based controller as shown in the block diagram in Fig. 4. Consequently, the friction and generator torques are calculated by linear relationships while the deviations are handled by the disturbance compensation torque, T_{comp}. Especially for low speeds and high load torques, and the start-up phase of the HIL system, deviations are relatively higher than the nominal operation point of the motor, generator and gear box. The torque-disturbance compensator ensures that the HIL simulator mimics the VAWT system successfully.
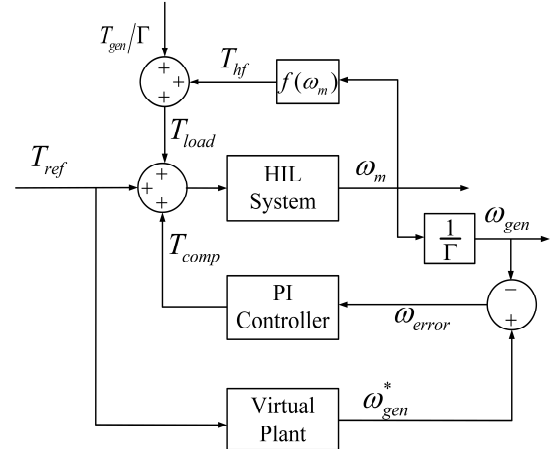

Fig. 4. Model following controller with a PI based disturbance compensator structure in the HIL system.

The results of the numerical (i.e. software-only) and the HIL simulations for a step change in the wind velocity are compared to confirm that the HIL simulator mimics the VAWT accurately. For this test, the generator torque is set to a value proportional to the speed, $T_{gen} = 0.1\,\omega_{gen}$ with the purpose of observing the dynamic effects only.

In Fig. 5, top plot shows the wind speed; the middle plot shows the generator speed obtained from numerical and the HIL

simulations; the bottom plot shows the error in the speed, which is the difference between the virtual plant and actual speeds in the HILS. Results confirm that the HIL simulator is capable of emulating the rotor inertia and mimicking the overall VAWT system. Parameters of the PI controller are given in Table II.
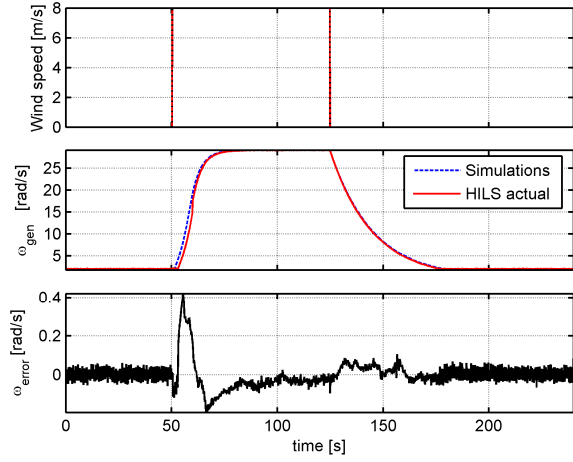

Fig. 5 The comparison of HIL and numerical simulations rotational speed responses for a step up and down wind speed.

TABLE II. PARAMETERS OF THE PI-CONTROLLER IN THE COMPENSATOR

Parameters of PID Controller and MPPT			
Parameter	Description	Value	Unit
K_P	Proportional gain	0.05	-
K_I	Integral gain	0.02	-

C. Power Electronics

In the HIL simulator, a PMSG and a passive diode rectifier are used as in the suggested VAWT system for electromechanical energy conversion. The passive diode rectifiers have disadvantages such as causing high harmonic currents, generator torque fluctuations and increasing the resistive loss, however they are low-cost and robust, and do not need a controller. In the PMSG-rectifier structure, output voltage is proportional to the rotor speed of the generator [20]. The highest output voltage prevails when the load current is zero, and the voltage output decreases as the current increases.

To determine how much the voltage drops for a given current and the generator speed, PMSG and the rectifier are modeled by a transformation from the 3-phase model to an equivalent DC machine model. In [21] and [22], a simplified DC equivalent model is proposed for PMSG-rectifier structure. The PMSG-rectifier model and the simplified equivalent DC model are shown in Fig. 6. In addition to the resistive voltage drop, armature reaction in the generator and overlapping currents in the rectifier during commutation intervals are also taken into account for the voltage drop calculations in this model. A relation is obtained between the 3-phase AC RMS values and DC potentials.
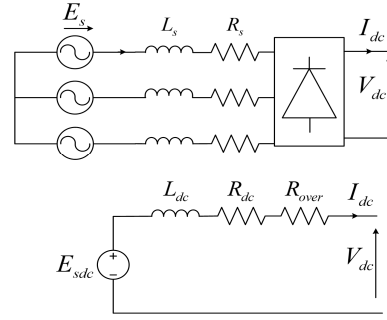

Fig. 6. PMSG-Rectifier and its simplified DC model.

In Fig. 6, E_s is electromotive force (EMF), L_s is phase inductance, R_s is the phase resistance of the PMSG, I_{dc} and V_{dc} are the average values of the DC current and voltage, respectively; E_{sdc}, L_{dc}, R_{dc} represents the correspondence values between the 3-phase AC model and the equivalent DC model. R_{over} term is added to the model to represent the average voltage drop due to the current commutation in the 3-phase passive diode bridge rectifier. This voltage drop from the current commutation is also explained in detail in [23]. The resistance, R_{over}, is calculated as follows:

$$R_{over} = \frac{3L_s p\omega_{gen}}{\pi} \tag{10}$$

where p is the number of pole pairs of the PMSG. For positive values of V_{dc}, ω_{gen} and I_{dc}, V_{dc} can be calculated as follows [21], [22]:

$$V_{dc} = \sqrt{E_{sdc}^{\,2} + \left(p\omega_{gen}L_{dc}I_{dc}\right)^2} - (R_{dc} + R_{over})I_{dc} \tag{11}$$

A simple test is carried out to verify the voltage drop model by running the PMSG with different speeds and currents. According to Fig. 7, the DC model predicts the actual voltage drop in the PMSG very well. The model variables for the PMSG-rectifier circuit and its DC equivalent model are provided in Table III.

TABLE III. PMSG AND DC MODEL VALUES

Variable	PMSG	DC Model
Flux	ϕ_s	$\phi_{dc} = 3\sqrt{6}\phi_s / \pi$
EMF	$E_s = \phi_s p\omega_{gen}$	$E_{sdc} = 3\sqrt{6}E_s / \pi$
Inductance	L_s	$L_{dc} = 18L_s / \pi^2$
Resistance	R_s	$R_{dc} = 18R_s / \pi^2$
$\phi_s = 0.106$ Vs/rad, $p = 6$, $L_s = 3.3$ mH, $R_s = 1.7$ Ω		

III. MAXIMUM POWER POINT TRACKING

In order to operate the VAWT at optimal power, the generator torque, T_{gen}, must be adjusted to balance the wind torque at the optimal rotor speed. The generator torque is proportional to the load current by a factor called the torque constant, K_t, which is obtained as 1.3 A/N-m here:
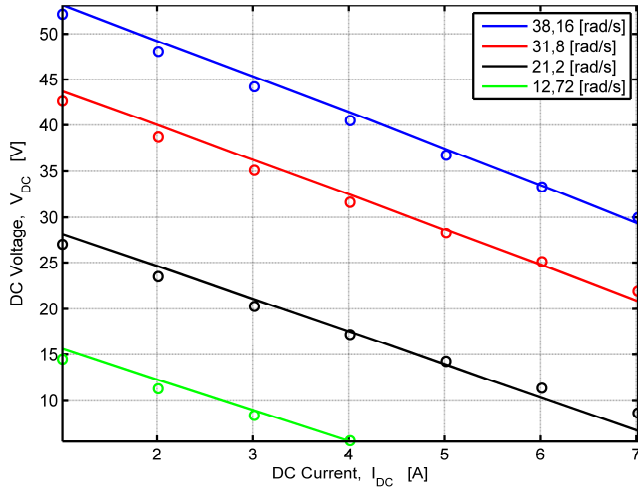
$$T_{gen} = K_t I_{dc} \tag{12}$$

Fig. 7. DC voltages with respect to the load current under different speed of PMSG that are represented by different colors. Solid lines represent the numerically calculated values, the circles show the experimental results.

The DC voltage of the PMSG-rectifier structure, V_{dc}, is a function of the generator speed, ω_{gen}, and the current, I_{dc}, as given in (11). Therefore, for each torque and generator speed pair, there is a unique pair of generator current and voltage, I_{dc} and V_{dc}. The output power, P_{dc}, is the product of the DC voltage and current, and may have a different maximum than the maximum power from the wind due to voltage and current characteristics of the generator and the power electronic circuit. Therefore, the overall characteristics of the system must be taken into account to find the maximum output power point of the VAWT system.

The plots of the wind and output power versus the rotor speed for a wind velocity of 8 m/s are shown in Fig. 8, where the maximum output power, $P_{dc,max}$, realizes for different speed than the maximum wind power, $P_{wind,max}$. The loss is relatively high in the low-speed / high-torque operating conditions for the PMSG, and hence $P_{dc,max}$ attains a maximum value for higher rotor speed than the speed at $P_{w,max}$. Obviously, losses and the efficiency characteristics result lower power output than the maximum available wind power.

In order to obtain the maximum power point, a control method is implemented based on an iterative tracking algorithm. The MPPT algorithm does not require the measurements of the wind velocity and the rotor speed. The incremental search for the optimum power output is based on the voltage and current measurements as described in [24]. The MPPT algorithm relies on the fact that the power output does not vary with voltage at the maximum point, i.e., the derivative of the power with respect to the voltage is zero:

$$\frac{dP_{dc}}{dV_{dc}} = \frac{d(V_{dc}I_{dc})}{dV_{dc}} = I_{dc} + V_{dc}\frac{dI_{dc}}{dV_{dc}} = 0 \implies \frac{dV_{dc}}{dI_{dc}} + \frac{V_{dc}}{I_{dc}} = 0 \quad (13)$$

According to (13), relative change in the voltage must be positive if the relative change in current is negative at the maximum power point or vice versa. Therefore, the MPPT algo-

rithm incrementally increases or decreases the current and compares with the change in the voltage to obtain the maximum power. The flowchart of the MPPT algorithm is presented in Fig. 9.
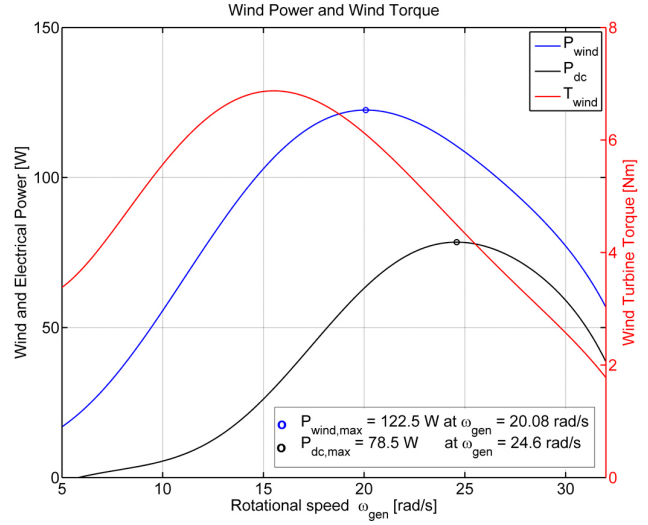

Fig. 8. Wind power P_{wind}, wind torque T_{wind} and electrical output power P_{dc} with respect to the rotational speed under 8 m/s wind speed. The power and the torque are associated with the left y-axis and the right y-axis respectively.
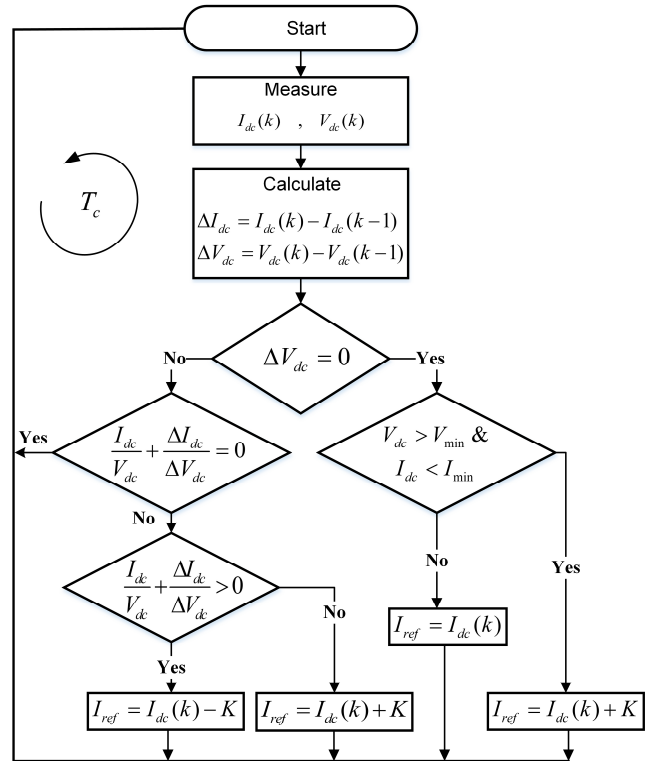

Fig. 9. Flow chart of the MPPT algorithm.

The algorithm starts with measuring the DC voltage and current, then it calculates the change in the voltage for a preset increment ($K > 0$) in the current. If the change in the voltage is

positive, it continues to increase the current until the voltage change is zero or negative; otherwise it decreases the current until the maximum power is reached. The sampling period of the control unit, T_c, is an important parameter that influences the performance of the algorithm significantly. The current step size, K, and the sampling period, T_c, need to be tuned to obtain fast response and small fluctuations around the target operating conditions.

IV. RESULTS

In this study, the proposed MPPT algorithm has been tested in the HIL simulator for step and sinusoidal wind conditions. Simulations are carried out by setting the sampling period of the HIL simulator to 1 ms. A parametric study is carried out to analyze the effects of the sampling period of the control unit (T_c) and the current increment size (K) on the energy output. Consequently, the parameters which provide the best performance in terms of energy output are determined as $T_c = 0.2$ s, $K = 0.5$ A.

First, the MPPT algorithm is tested for a step change in the wind velocity, which is depicted with respect to time in the top plot in Fig. 10. Corresponding plots for the generator (rotor) speed, ω_{gen}, electrical output power P_{dc}, current, I_{dc} and the DC voltage V_{dc}, are also shown in Fig. 10. Numerical simulations and HIL simulator results agree well. Simulations predict slightly higher currents, lower rotor speeds and voltage outputs than the HIL simulator, but power outputs of both simulations are close. Fluctuations due to the MPPT algorithm are present in the current and the voltage in both simulations, however, slightly larger in the HIL simulations than in the numerical ones. Results are summarized in Table IV.

TABLE IV. COMPARISON OF ELECTRICAL OUTPUT POWERS UNDER DIFFERENT WIND SPEED

Wind Speed [m/s]	Electrical output power P_{dc} under step change in steady state		
	Theoretically Calculated Power [W]	Numerical (Software-only) Simulation Power [W]	HILS Power [W]
6	36.75	32 – 33	25 - 40
8	78.46	70 – 71	65 - 86
10	137.7	129 – 133	110 – 150

Although the average measured power in the HILS is less than the calculated power in the numerical simulation, the HILS power oscillates and occasionally reaches higher power values than the theoretical maximum power values by using the kinetic energy stored in the rotor. In the HIL system, the MPPT algorithm generates a reference current to track its optimal value. However, tracking the reference current does not cease at the optimum value, and continues with overshoots and undershoots. During this time, energy stored in the inertia is extracted, and hence higher instantaneous power outputs than the theoretical maximum are observed.

The MPPT algorithm is also tested for a sinusoidal wind velocity with frequencies of 0.1 Hz and 0.05 Hz, and the results are represented in Fig. 11. Results indicate that the HIL simulator and the numerical model agree well. In both cases, the MPPT algorithm leads to a power generation with a slight phase difference between the wind and the power output signals.
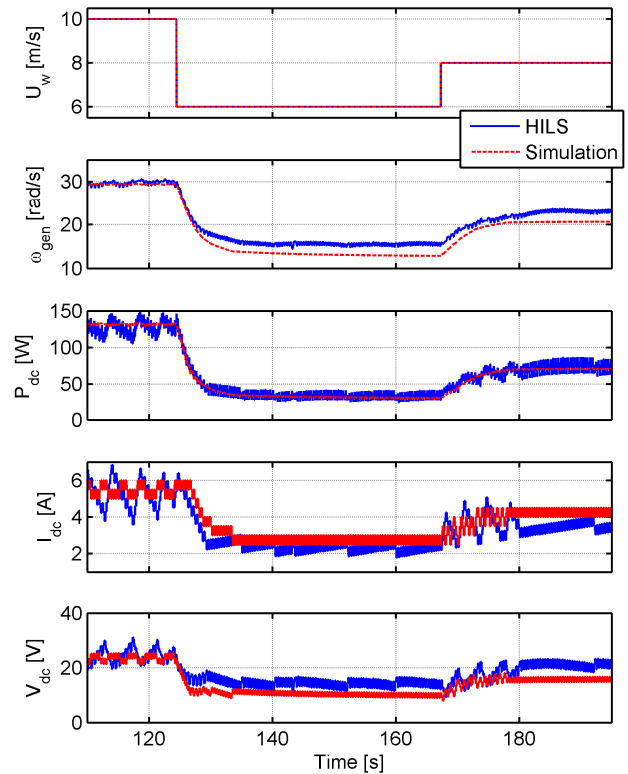

Fig. 10. Numerical simulation and HILS results for the step down and up wind speed.

V. CONCLUSION

The HIL system performs satisfactorily, emulates the overall VAWT system realistically, and allows controlled experiments for ideal wind conditions which are difficult to obtain in actual experiments with the turbine. The HIL simulations are especially useful to test the performance of power electronic components and control designs. According to the HIL simulations, the electrical properties of the PMSG generator and rectifiers may lead to lower power outputs than the available power in the wind. As a part of future work, alternative generators can be tested to obtain ideal generator for a given rotor and wind conditions. Moreover, active rectification can be carried out to mitigate the harmonics which have no contribution to the active power and decreases the efficiency in the case of a passive rectifier.

For the control design, we implemented the MPPT algorithm and observed that power fluctuations in the HIL simulator are higher than the ones observed with the numerical model. The algorithm leads to overshoots and undershoots, which correspond to use and storage of the kinetic energy in the rotor due to delay introduced by the sampling time of the algorithm.

Adaptive increments in current and sampling times can be used for power tracking with smaller fluctuations and faster responses.
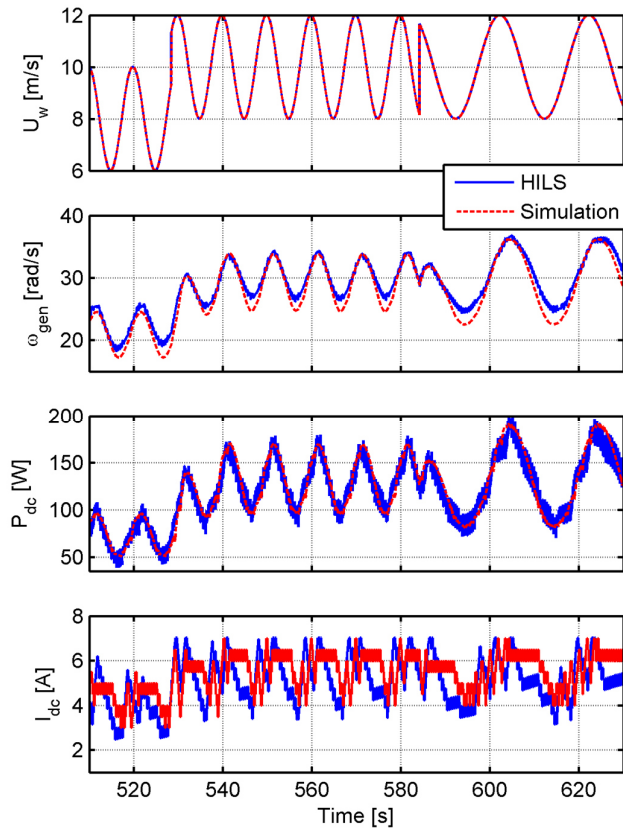

Fig. 11. Numerical simulation and HILS results for the sinusoidal wind speed.

REFERENCES

[1] Da Rosa, A. V. (2005). Fundamentals of renewable energy processes. Academic Press.

[2] Eriksson, S., Bernhoff, H., & Leijon, M. (2008). Evaluation of different turbine concepts for wind power. Renewable and Sustainable Energy Reviews, 12(5), 1419-1434.

[3] Muljadi, E., Pierce, K., & Migliore, P. (2000). Soft-stall control for variable-speed stall-regulated wind turbines. Journal of Wind Engineering and Industrial Aerodynamics, 85(3), 277-291.

[4] Burton, T., Sharpe, D., Jenkins, N., & Bossanyi, E. (2001). Wind energy handbook. John Wiley & Sons.

[5] Jogendra Singh Thongam and Mohand Ouhrouche (2011). MPPT Control Methods in Wind Energy Conversion Systems, Fundamental and Advanced Topics in Wind Power, Dr. Rupp Carriveau (Ed.), ISBN: 978-953-307-508-2, InTech, Available from: http://www.intechopen.com/books/fundamental-and-advancedtopics- in-wind-power/mppt-control-methods-in-wind-energy-conversion-systems.

[6] Kot, R., Rolak, M., & Malinowski, M. (2013). Comparison of maximum peak power tracking algorithms for a small wind turbine. Mathematics and Computers in Simulation, 91, 29-40.

[7] Narayana, M., Putrus, G. A., Jovanovic, M., Leung, P. S., & McDonald, S. (2012). Generic maximum power point tracking controller for small-scale wind turbines. Renewable Energy, 44, 72-79.

[8] Koutroulis, E., & Kalaitzakis, K. (2006). Design of a maximum power tracking system for wind-energy-conversion applications. Industrial Electronics, IEEE Transactions on, 53(2), 486-494.

[9] Steurer, M., Bogdan, F., Ren, W., Sloderbeck, M., & Woodruff, S. (2007, June). Controller and power hardware-in-loop methods for accelerating renewable energy integration. In Power Engineering Society General Meeting, 2007. IEEE (pp. 1-4). IEEE.

[10] Bouscayrol, A. (2008, June). Different types of hardware-in-the-loop simulation for electric drives. In Industrial Electronics, 2008. ISIE 2008. IEEE International Symposium on (pp. 2146-2151). IEEE.

[11] Neammanee, B., Sirisumrannukul, S., & Chatratana, S. (2007). Development of a wind turbine simulator for wind generator testing. International Energy Journal, 8(1), 21-28.

[12] Li, H., Steurer, M., Shi, K. L., Woodruff, S., & Zhang, D. (2006). Development of a unified design, test, and research platform for wind energy systems based on hardware-in-the-loop real-time simulation. Industrial Electronics, IEEE Transactions on, 53(4), 1144-1151.

[13] SOng, S. H., Jeong, B. C., Lee, H. I., Kim, J. J., Oh, J. H., & Venkataramanan, G. (2005, March). Emulation of output characteristics of rotor blades using a hardware-in-loop wind turbine simulator. In Applied Power Electronics Conference and Exposition, 2005. APEC 2005. Twentieth Annual IEEE (Vol. 3, pp. 1791-1796). IEEE.

[14] Muntean, N., Tutelea, L., Petrila, D., & Pelan, O. (2011, September). Hardware in the loop wind turbine emulator. In Electrical Machines and Power Electronics and 2011 Electromotion Joint Conference (ACEMP), 2011 International Aegean Conference on (pp. 53-58). IEEE.

[15] Lin, D., Zhou, P., & Cendes, Z. J. (2009). In-depth study of the torque constant for permanent-magnet machines. Magnetics, IEEE Transactions on, 45(12), 5383-5387.

[16] Tsai, M. C., Chiu, I. F., & Cheng, M. Y. (2004, January). Design and implementation of command and friction feedforward control for CNC motion controllers. In Control Theory and Applications, IEE Proceedings- (Vol. 151, No. 1, pp. 13-20). IET.

[17] Stajic, D., Peric, N., & Deur, J. (1999). Friction compensation methods in position and speed control systems. In Industrial Electronics, 1999. ISIE'99. Proceedings of the IEEE International Symposium on (Vol. 3, pp. 1261-1266). IEEE.

[18] Saglam, C. O., Baran, E. A., Nergiz, A. O., & Sabanovic, A. (2011, April). Model following control with discrete time SMC for time-Delayed bilateral control systems. In Mechatronics (ICM), 2011 IEEE International Conference on (pp. 997-1002). IEEE.

[19] Wu, J. C., Su, K. H., & Cheng, M. Y. (2010, November). Friction and disturbance compensation for speed control of servo control systems. In IECON 2010-36th Annual Conference on IEEE Industrial Electronics Society (pp. 1890-1895). IEEE.

[20] Lo, K. Y., Chen, Y. M., & Chang, Y. R. (2011). MPPT battery charger for stand-alone wind power system. Power Electronics, IEEE Transactions on, 26(6), 1631-1638.

[21] Sareni, B., Abdelli, A., Roboam, X., & Tran, D. H. (2009). Model simplification and optimization of a passive wind turbine generator. Renewable Energy, 34(12), 2640-2650.

[22] Tran, D. H., Sareni, B., Roboam, X., & Espanet, C. (2010). Integrated optimal design of a passive wind turbine system: an experimental validation. Sustainable Energy, IEEE Transactions on, 1(1), 48-56.

[23] Mohan, N., & Undeland, T. M. (2007). Power electronics: converters, applications, and design. John Wiley & Sons.

[24] Hosseini, S. H., Farakhor, A., & Haghighian, S. K. (2013, November). Novel algorithm of maximum power point tracking (MPPT) for variable speed PMSG wind generation systems through model predictive control. In Electrical and Electronics Engineering (ELECO), 2013 8th International Conference on (pp. 243-247). IEEE.